

DESIGN OF A TRIPLE CROSSED FLEXURE PIVOT WITH MINIMIZED PARASITIC SHIFT

E. Thalmann*

Micromechanical and Horological Design Laboratory
(Instant-Lab), Institute of Microengineering,
École Polytechnique Fédérale de Lausanne (EPFL),
Microcity, Rue de la Maladière 71b,
CH-2000 Neuchâtel, Switzerland
etienne.thalmann@epfl.ch

S. Henein,

Micromechanical and Horological Design Laboratory
(Instant-Lab), Institute of Microengineering,
École Polytechnique Fédérale de Lausanne (EPFL),
Microcity, Rue le la Maladière 71b,
CH-2000 Neuchâtel, Switzerland
simon.henein@epfl.ch

ABSTRACT

Thanks to their absence of play, absence of contact friction and possible monolithic fabrication, flexure pivots offer advantages over traditional bearings in small-scale, high accuracy applications and environments where lubrication and wear debris are proscribed. However, they typically present a so-called parasitic center shift that deteriorates their rotational guidance accuracy. Existing solutions addressing this issue have the drawbacks of reducing angular stroke, prohibiting planar design, or introducing overconstraints or underconstraints. This article introduces a new triple crossed flexure pivot called TRIVOT that has a reduced parasitic shift without overconstraints nor internal mobility while allowing either optimal stress distribution in the flexures or a planar design. The new architecture also makes it possible to place the center of rotation outside of the physical structure, which is not the case with traditional bearings. Based on finite element simulations, we show that the parasitic shift is reduced by one order of magnitude in comparison to the widely used crossed flexure pivot. We also derive and validate formulas for the rotational stiffness and angular stroke limit of the TRIVOT for given dimensions and material, which are valuable for its dimensioning towards practical applications. We expect this new pivot to become a competitive alternative to the crossed flexure pivot for applications where high accuracy and compactness are required.

Keywords: Compliant mechanism, Flexure pivot, Flexure hinge, Parasitic shift, Accuracy, Remote center of compliance.

1 INTRODUCTION

Flexure pivots, which use the elastic deformation of slender beams to guide a rotational motion, are attractive alternatives to traditional bearings for a wide range of applications where high accuracy and absence of contact friction are desired. Such applications include micromanipulation devices [1, 2, 3], aerospace mechanisms [4, 5], medical devices [6, 7] and watch-making [8, 9, 10]. Flexure pivots, however, face limitations in comparison to bearings such as a parasitic shift of their rotation axis, limited stroke, complex designs, overconstraints or internal degrees-of-freedom. For instance, the Crossed Flexure Pivot (CFP) (a.k.a. cross-spring pivot) introduced by Wittrick [11] can either have a minimal parasitic shift, a planar design, or the maximal admissible stroke for given leaf springs. Other pivots achieve a large stroke, a very small parasitic shift and a planar design by using serial arrangements of flexures, such as the “Butterfly” pivot [4] or the multi-stage compound radial flexure [12]. These architectures however have the drawback of having internal (redundant) degrees-of-freedom that can be excited by vibrations or need external slaving mechanisms to be suppressed [13, 14]. Alternatively, the “GIFP” pivot [9, 15] allows to optimally distribute the stress in the flexures and significantly reduce the parasitic

*Address all correspondence to this author.

shift in comparison to the CFP, but at the expense of compactness. The “co-RCC” pivot [16, 17] presents an interesting way of reducing the parasitic center shift while having a planar design but the remaining center shift is not negligible [9]. Other solutions exist to tackle the issue of parasitic shift while maximizing angular stroke or having a planar design, but they are either overconstrained [18] or have additional elasticity at one extremity [19].

In this paper, we present a new TRIPLe crossed flexure piVOT (TRIVOT) whose design theoretically cancels its parasitic center shift, regardless of the crossing ratio of its flexures, allowing to either achieve the maximum angular stroke for given flexures or a planar design. Furthermore, the center of rotation can be placed outside of the physical structure, a property called *Remote Center of Compliance* (RCC) [14, 20] that could previously only be achieved with a parasitic shift [21] or with serial compensations that add complexity or internal degrees-of-freedom [1, 12, 22]. We first give a detailed description of the TRIVOT design and its variants (Section 2). We then quantify its parasitic shift using the finite element method (FEM) and use the CFP as benchmark for comparison (Section 3.1). Finally, we derive and validate formulas for the rotational stiffness (Section 3.2) and admissible angular stroke (Section 3.3) of the TRIVOT.

2 DESIGN OF THE TRIVOT FLEXURE PIVOT

2.1 General kinematics

In order to describe the design of the TRIVOT, we give a step-by-step explanation based on the two-dimensional kinematic diagram in Fig. 1:

- (a) The design consists of a “mobile body” rotating with respect to a “fixed body” about a point O , which we call the center of the mechanism.
- (b) Three parallel kinematic chains connect the mobile body to the fixed one. Each chain consists of a “main connecting rod”, with a pivot joint at each extremity, in series with a slider joint. The connecting rods all have the same length and are attached to the fixed body at the same distance from point O . The connecting rods each form the same angle with a segment joining their outer pivot (attached to the slider joint) to point O . It follows that there exists a “neutral” position of the mobile body in which the axes of the connecting rods are concurrent at point O (Fig. 1d). The axes of the sliders are parallel to the segments joining point O to the outer pivot of the connecting rod to which they are respectively connected. This enables the distance between the mobile body and point O to stay constant while the structure rotates, which is key to cancelling the parasitic center shift.
- (c) The “intermediate links” between the connecting rods and the mobile body are connected in pairs by two kinematic

chains, each consisting of a slider in series with a pivot. The sliding axis of each chain forms the same angles with the two adjacent slider axes. The result of this coupling can be seen in the shape of two isosceles trapezoids formed by the mobile body and the sliding axes. This ensure that the sliders of same type always perform the same motion. It follows that the motion of the intermediate links is concentric with respect to O .

- (d) As a result of this geometry, the mobile body only has one degree-of-freedom (DOF): a pure rotation about point O described by the angle θ , see animation [23]. In comparison to an architecture without intermediate links like the CFP, the sliders absorbs the parasitic motion of the connecting rod’s mobile end, hence cancelling it.

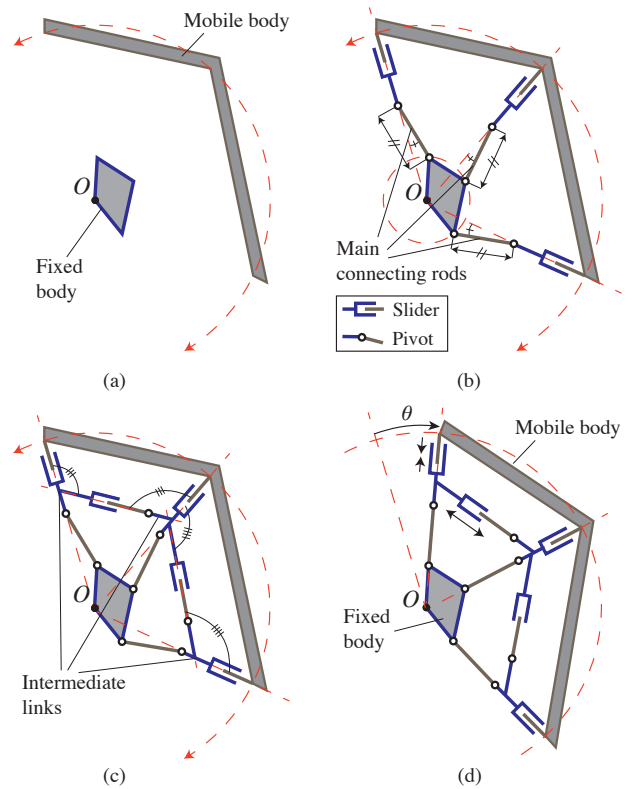


FIGURE 1: Step-by-step description of the TRIVOT kinematics. Animation is available [23].

Since there are no internal degrees-of-freedom, Grübler’s formula for planar linkages [24] shows that the mobility $M = 1$ is obtained without overconstraint:

$$M = \sum_{i=1}^j f_i - 3(j - N + 1) = 13 - 3(13 - 10 + 1) = 1 \quad (1)$$

In this formula, $N = 10$ is the number of bodies and $j = 13$ is the number of joints with each a DOF $f_i = 1$. Note that the fixed and mobile parts of the pivot are interchangeable.

2.2 Symmetrical design

In order to have a symmetrical architecture, we modified the general design depicted in Fig. 1c as follows (Fig. 2):

1. The connecting rods were fixed at the vertices of an equilateral triangle.
2. An additional kinematic chain was added between the intermediate links.
3. The neutral position was chosen as nominal.

This symmetry has the advantages of improving the mass distribution relative to O and reducing the differences in radial support stiffness in the flexure implementation. Note that an extra DOF was added to avoid overconstraining the mechanism with the added kinematic chain.

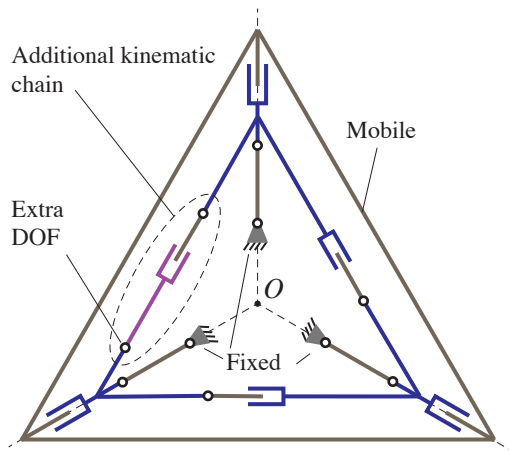


FIGURE 2: Symmetrical TRIVOT design.

To facilitate flexure implementation, we modified the design further, by replacing the slider joints with combinations of pivot-pivot connecting rods (Fig. 3a):

4. The sliders between the intermediate links and the mobile body were replaced with parallel connecting rods whose parabolic motion closely approximates translations for small displacements [14].
5. The slider-pivot kinematic chains were replaced with connecting rods perpendicular to the sliding axis whose motion closely approximates a pin-in-slot joint for small displacements.

For small displacements, this pivot closely approximates a pure rotation about O and the motion of the extra DOF is infinitesimal, see Fig. 3b and animation [25].

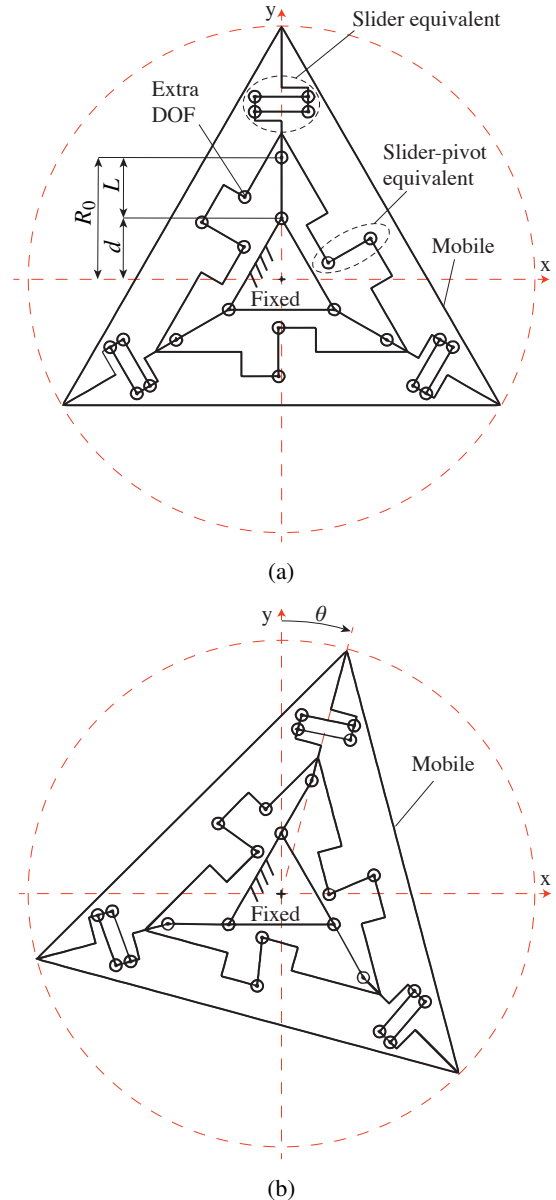
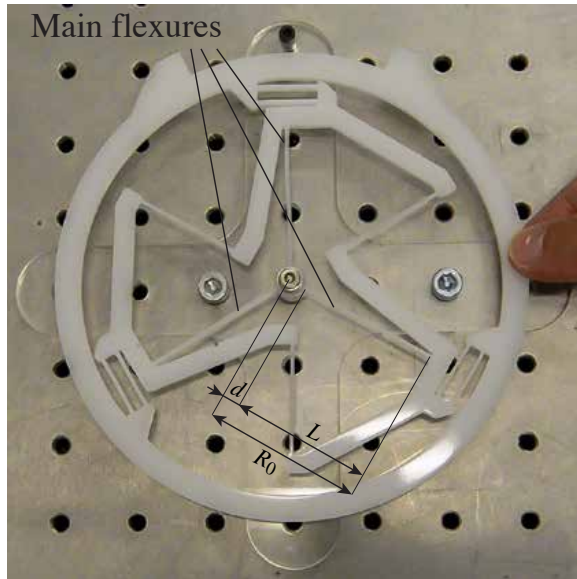


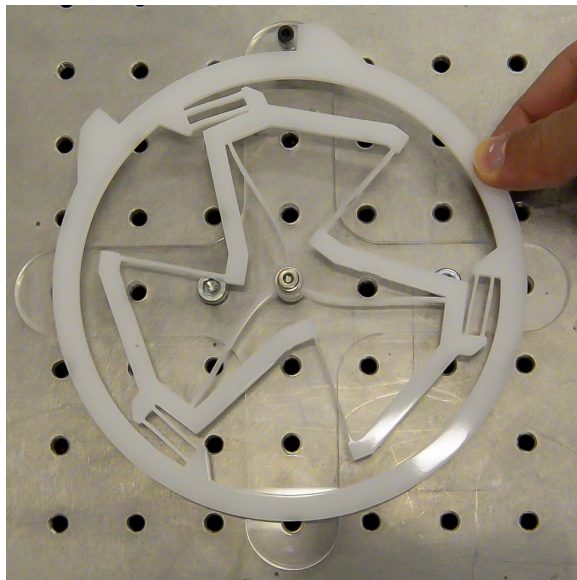
FIGURE 3: Kinematic diagram of the symmetrical TRIVOT with $\delta > 0$ in (a) nominal position and (b) rotated by angle θ . Animation is available [25].

The connecting rods can then conveniently be embodied by leaf springs or rigid bars with notch flexure hinges at each extremity, which have equivalent kinematic behavior [14, 26]. We

carried out such implementation using leaf springs in the mock-up of Fig. 4. This setup demonstrates that the design behaves qualitatively as a pivot, see video [27]. Note that since the part needed no assembly, we omitted the extra DOF, assuming that there is enough flexibility in the system to release the overconstraint.



(a)



(b)

FIGURE 4: Mock-up of the planar TRIVOT with $\delta = 0.1$ and an outer diameter of 150 mm fabricated by laser cutting a 5 mm thick Polyoxymethylene (POM) sheet: (a) nominal position (b) rotated by 22 degrees. Video is available [27].

2.3 Crossing ratio δ of the flexures

Since the main flexures (Fig. 4a) perform the main motion during the rotation of the TRIVOT, their dimensions and crossing ratio determine the main properties of the pivot. Indeed, their deformation is of order of the rotation angle θ of the pivot whereas the deformation of the other “secondary” flexures is of order θ^2 . The kinematic boundary conditions of these main flexures are similar to those of the CFP [11, 28], hence we define the ratio at which they cross in an analogous way with the dimensionless ratio $\delta = d/L$ [29]. Here, L is the length of the flexures and d is the distance from their crossing point to their extremity attached to the body 1, see Fig. 4a. These distances can be determined equivalently in the ideal kinematic diagrams, see Fig. 3a. The signs of d and L are defined with respect to the direction from the center O to the extremity of the flexure attached to the intermediate link. We then categorize TRIVOT architectures according to the sign of δ :

- When $\delta > 0$, d and L are of same sign and the main flexures (respectively main connecting rods) cross virtually outside of their physical structure (Fig. 3a). This has the benefits of a planar design (Fig. 4), which is advantageous for compactness and manufacturing, and potentially a RCC configuration (Fig. 1).
- When $-0.5 \leq \delta \leq 0$, d and L are of opposite sign and the main flexures (respectively main connecting rods) cross physically at the center of the mechanism (Fig. 5). This has the benefit of better distributing the stress within the flexures [30] but requires a physical implementation allowing the flexures to cross. An example of such an architecture using three planes is depicted in Fig. 6.
- When $\delta < -0.5$, the positions of the fixed and mobile bodies are exchanged with respect to the center O . It is assumed that the pivot behaves similarly to the case where δ is substituted with $\delta' = -1 - \delta$ [30].

3 MECHANICAL PROPERTIES

The main advantage of the TRIVOT in comparison to other crossed flexure pivots is its reduced parasitic center shift. Here, we quantify this effect using FEM and compare it to our benchmark, the CFP. We also provide expressions for two other properties of flexure pivots that differ from ideal pivots and need to be taken into account when dimensioning: the rotational stiffness and the angular stroke limit.

3.1 Parasitic center shift

Figure 7 compares the parasitic shift of the TRIVOT and CFP for different values of the crossing ratio δ . In order to compare architectures with similar external diameter, we chose to keep $R_0 = L(\delta + 1)$ constant in all results (see Fig. 4a and

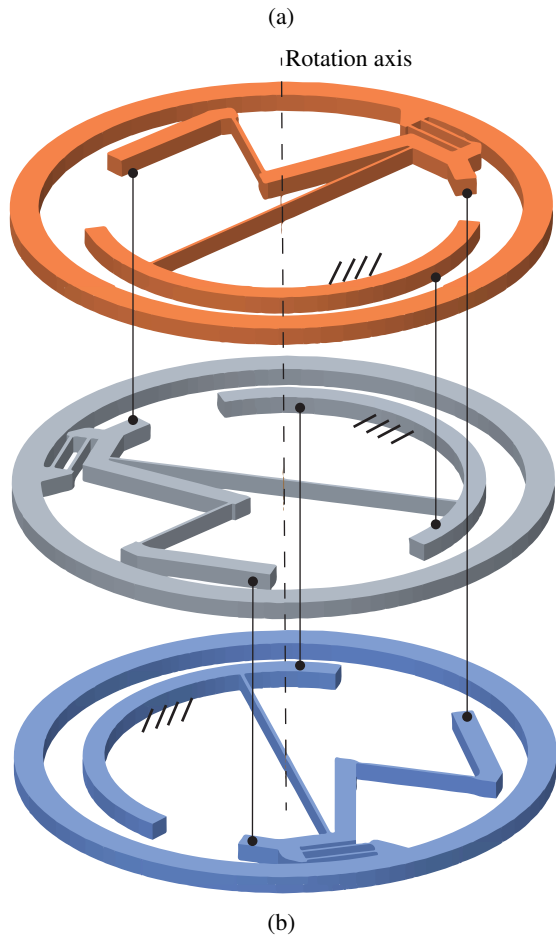
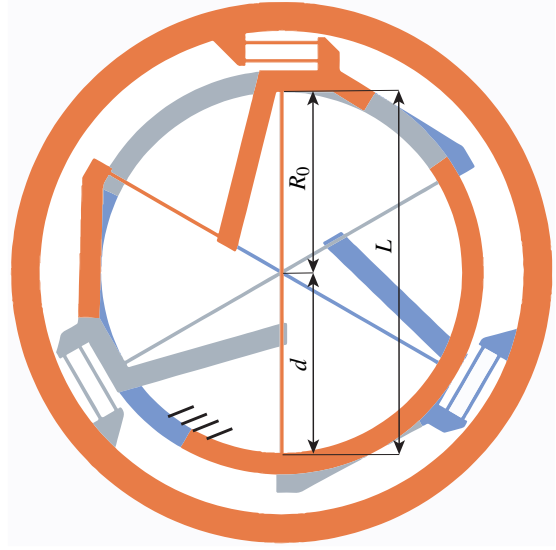
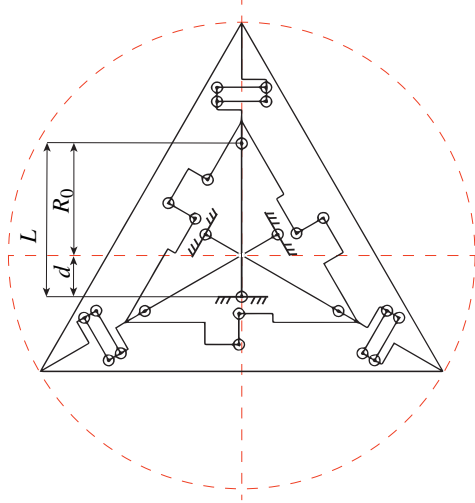


FIGURE 5: Kinematic diagram of the symmetrical TRIVOT with $-0.5 \leq \delta \leq 0$.

Fig. 6a). The norm of the parasitic center shift $D = \sqrt{D_x^2 + D_y^2}$ is compared for a 15 degree rotation of the pivots. For the TRIVOT, D_x and D_y are the components along the xy -coordinates depicted in Fig. 3 of a point on the mobile body located at point O in the nominal position. For the CFP, the parasitic shift was computed using [31, Eq. (17.1)-(17.2)], assuming orthogonal flexures. To make the results independent of size, they are normalized by R_0 using $\tilde{D} = \frac{D}{R_0}$. The thickness h of the main flexures is constant for all designs and satisfies $\tilde{h} = \frac{h}{R_0} = 0.02$. We chose this value to have flexure aspect ratios that are compatible with standard micromanufacturing techniques such as wire electro-discharge machining (EDM).

For the given dimensions and rotation angle, the results show that the parasitic shift of the TRIVOT does not exceed 0.13% of R_0 whereas the CFP is always above these values, except for a narrow region of δ around -12.7% that is known to minimize its center shift [29]. For $\delta = -0.5$, which is known to optimize the stress distribution in the flexures [30] (and hence maximize the angular stroke, see Section 3.3), the parasitic shift of the TRIVOT is more than ten times smaller than that of the CFP. For $\delta > 0$, which permits planar designs and RCC properties, the center shift of the TRIVOT is also reduced by one order of magnitude in comparison to the CFP.

The parasitic center shift of the TRIVOT was computed using the commercial FEM software ANSYS [32], by applying a rotation on the mobile body and computing the motion of its center of mass (Fig. 8a). The TRIVOT was meshed with hexahedral SOLID186 elements refined on the flexures such that there are three elements across their thickness, five along their height and a number of elements along the length conferring them a square face (Fig. 8b).

FIGURE 6: Flexure implementation of the TRIVOT with crossed flexures ($-0.5 \leq \delta \leq 0$): (a) top view (b) exploded view. The lines with points at their extremities show the connections between rigid bodies across the three planes.

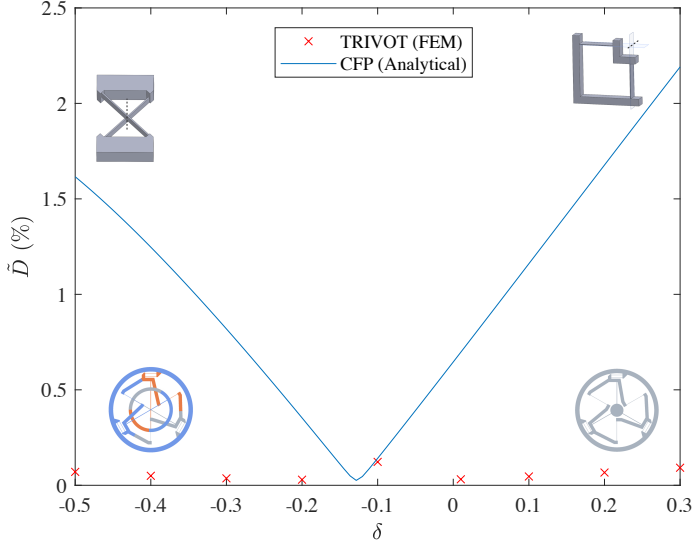


FIGURE 7: Normalized parasitic center shift of the TRIVOT and CFP versus crossing ratio of the flexures.

3.2 Rotational stiffness

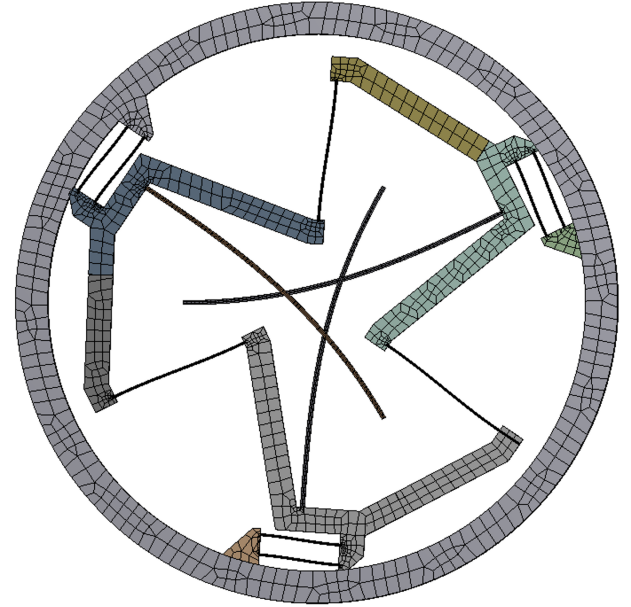
In the case where the TRIVOT is subjected to pure torque, i.e., we assume no external loads, the main flexures can be modelled as cantilever beams subject to a pure bending moment with a prescribed rotation θ at their free end. The same kinematic boundary conditions can be found for the CFP. Hence, we can adapt the formula for the rotational stiffness of the CFP [30, Eq. (12)] to the case with three flexures:

$$k = \frac{12EI}{L} (3\delta^2 + 3\delta + 1) \quad (2)$$

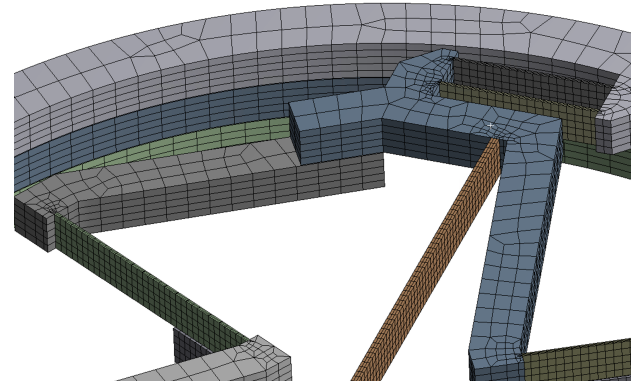
Here, E and I are respectively Young's modulus for the flexures and their area moment of inertia. Note that the angle between the flexures does not appear in this formula, which makes it applicable to any TRIVOT configuration. In order to provide results that are independent from size and material, the rotational stiffness was normalized as follows:

$$\tilde{k} = \frac{R_0}{EI} k = 12 (\delta^2 + 3\delta + 1) (\delta + 1) \quad (3)$$

In order to validate Eq. (3) and to show the influence of the flexures' crossing ratio on the stiffness of the TRIVOT, analytical and FEM results for \tilde{k} versus δ are plotted in Fig. 9. The FEM stiffness was obtained with the model described in Section 3.1, by computing the reaction torque on the fixed frame for a 1 degree rotation of the mobile body. The analytical results match the FEM results with less than 3% discrepancy, thus providing validation for our formula. For comparison, Fig. 9 also displays



(a)



(b)

FIGURE 8: Finite element model of the TRIVOT: (a) 25 degree rotation with $\delta = 0.4$ (b) close-up view of the mesh.

the normalized stiffness of the CFP, namely, 2/3 of the TRIVOT stiffness.

Remark 3.1. The rotational stiffness given by Eq. (3) is only valid for small rotations within approximately ± 10 degrees. For larger deformations, nonlinear effects can have a significant impact. It is indeed known that the rotational stiffness of crossed flexures varies with the rotation angle [33, 34]. Additionally, the secondary flexures of the TRIVOT undergo a deformation that is of second order of the main rotation resulting in a stiffening of the pivot as it moves away from equilibrium [19, 16].

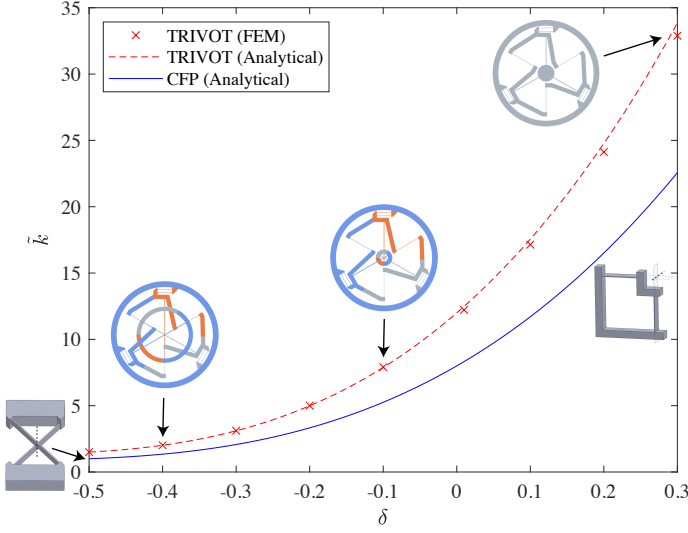


FIGURE 9: Normalized rotational stiffness of the TRIVOT and CFP versus crossing ratio of the flexures.

3.3 Admissible angular stroke

As in Section 3.2, when the TRIVOT is subjected to pure bending moment, the stresses in the flexures follow the same distribution as in the CFP. The same equations thus apply and the maximum angular stroke of the TRIVOT for a given admissible stress σ_{adm} in the material is [30, Eq. (23)-(27)]:

$$\theta_{max} = \frac{\sigma_{adm}L}{Eh(2+3\delta)} \quad (4)$$

In order to validate this formula and to show the influence of the flexures' crossing ratio on the admissible stroke of the TRIVOT, Fig. 10 shows FEM and analytical values of θ_{max} versus δ for an example of implementation. We chose a material with an admissible elastic strain $\epsilon_{adm} = \frac{\sigma_{adm}}{E} = 0.4\%$, which can typically be reached with steel alloys, titanium alloys, polymers, glass or silicon [35, Table B.14] [36,37]. As previously, R_0 and h are kept constant and satisfy $\tilde{h} = \frac{h}{R_0} = 0.02$. Equation 4 can now be rewritten in terms of our dimensionless parameters :

$$\theta_{max} = \frac{1}{\epsilon_{adm} \tilde{h} (1+\delta)(2+3\delta)} \quad (5)$$

The FEM results are based on the von Mises stress in the main flexures for an applied rotation on the mobile body using the model described in Section 3.1. The analytical results match the FEM results with less than 5% discrepancy for $\delta \geq -0.35$, thus providing validation for our formula.

For $\delta \leq -0.35$, the admissible rotation angles become large ($\theta_{max} > 20$ degrees) and the parasitic rotation caused by the

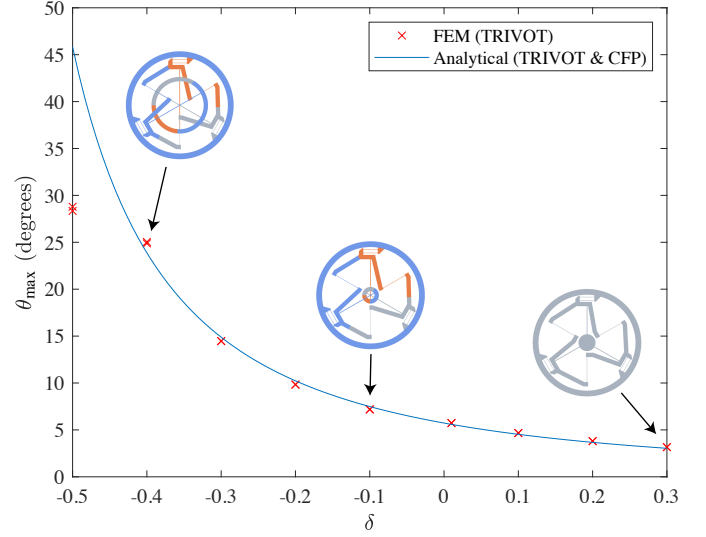


FIGURE 10: Admissible angular stroke of a TRIVOT and CFP with $\epsilon_{adm} = 0.4\%$ and $\tilde{h} = 0.02$ versus crossing ratio of the flexures.

asymmetry of our implementation with respect to the plane of rotation is no longer negligible (three different superimposed levels in Fig. 6b). This parasitic rotation about an axis perpendicular to the main rotation axis subjects the flexures to additional torsion and bending stresses. For crossing ratios around $\delta = -0.5$, Fig. 10 shows that this significantly reduces the admissible angular stroke. This issue can however be solved by using a symmetrically stacked architecture by, for instance, using five levels (similarly to the CFP with three flexures [38, Fig. 4]) or by using interlocked lattice flexures [39]. It is assumed that in that case the admissible stroke would be close to the predictions of Eq. (5).

Remark 3.2. Bear in mind that the admissible stroke of the TRIVOT depends on the material and dimensions. For instance, the architectures with $\delta > 0$ in Fig. 10 have a flexure aspect ratio $L/h < 50$ that could be increased without compromising manufacturability in order to reach greater angular stroke. The mock-up in Fig. 4 also achieves a larger rotation angle due to the high admissible strain of its material ($\epsilon_{adm} \approx 2.3\%$).

Remark 3.3. Since the TRIVOT does not have an axial symmetry in the plane of rotation, its behavior is different for clockwise and counter-clockwise motions. This asymmetry however only concerns the secondary flexures, whose deformation is of second order of the main rotation θ . It is hence assumed that the consequences of this asymmetry will only be apparent for large deformations or in the study of nonlinear effects, see Remark. 3.1. This assumption is confirmed in Fig. 10 where the FEM results for clockwise and counter-clockwise rotations are displayed, showing only a slight difference for large admissible strokes ($\theta_{max} > 20$ degrees).

TABLE 1: Qualitative comparison between TRIVOT and CFP properties.

Flexure pivot	Reduced parasitic shift	Maximized angular stroke	Planar design	RCC
TRIVOT with $\delta = -0.5$	Yes	Yes	No	No
TRIVOT with $\delta > 0$	Yes	No	Yes	Yes
CFP with $\delta = -0.5$	No	Yes	No	No
CFP with $\delta = -0.127$	Yes	No	No	No
CFP with $\delta > 0$	No	No	Yes	Yes

CONCLUSION

In this article, we presented the design of a novel flexure pivot whose ideal kinematics achieve a pure rotation without overconstraint. We showed different configurations, characterized by the crossing ratio of the main flexures, allowing to either maximize the admissible angular stroke for given flexures or to have a planar design. We demonstrated that these properties could be achieved while maintaining a very small parasitic center shift, which is not the case with our CFP benchmark (see comparison in Table 1). These improvements nevertheless increase complexity, with six times more flexures than the CFP and a fabrication over at least three levels in the configuration with crossing flexures. Overall, the TRIVOT design is an improvement over other flexure pivots that achieve similar properties but have the drawback of having either overconstraints, internal degrees-of-freedom or elasticity in one of the bodies.

By solving the issue of parasitic center shift, which is a common obstacle to the replacement of traditional bearings with flexure pivots, the TRIVOT paves the way to new applications that could benefit from its absence of play, contact friction, wear, polluting debris, need for lubrication, and its possible monolithic fabrication. Additionally, the TRIVOT provides a new way of implementing a remote center of rotation, which is not possible with traditional bearings and required in numerous applications. Our future research directions include the experimental validation of the results presented here, the analysis of the stiffness nonlinearity of the TRIVOT and a dimensioning for a mechanical watch oscillator application.

ACKNOWLEDGMENT

We thank Ilan Vardi for his constructive criticism and careful review of the manuscript. We also thank Arnaud Maurel for his assistance in fabricating the mock-up in Fig. 4.

REFERENCES

- [1] Helmer, P., 2006. “Conception systématique de structures cinématiques orthogonales pour la microrobotique”. PhD thesis, EPFL, DOI: 10.5075/epfl-thesis-3365.
- [2] Richard, M., and Clavel, R., 2010. “A new concept of modular kinematics to design ultra-high precision flexure-based robots”. In *ISR 2010 (41st International Symposium on Robotics) and ROBOTIK 2010 (6th German Conference on Robotics)*, pp. 1–8.
- [3] Verotti, M., Dochshyanov, A., and Belfiore, N. P., 2017. “A Comprehensive Survey on Microgrippers Design: Mechanical Structure”. *Journal of Mechanical Design*, **139**(6), May, p. 060801, DOI: 10.1115/1.4036351.
- [4] Henein, S., Spanoudakis, P., Droz, S., Myklebust, L. I., and Onillon, E., 2003. “Flexure Pivot for Aerospace Mechanisms”. In *Proceedings of the 10th ESMATS*.
- [5] Huo, T., Yu, J., and Zhao, H., 2020. “Design of a kinematic flexure mount for precision instruments based on stiffness characteristics of flexural pivot”. *Mechanism and Machine Theory*, **150**, Aug., p. 103868, DOI: 10.1016/j.mechmachtheory.2020.103868.
- [6] Zanaty, M., Fussinger, T., Rogg, A., Lovera, A., Lambelet, D., Vardi, I., Wolfensberger, T. J., Baur, C., and Henein, S., 2019. “Programmable Multistable Mechanisms for Safe Surgical Puncturing”. *Journal of Medical Devices*, **13**(2), June, DOI: 10.1115/1.4043016.
- [7] Fifanski, S. K., 2020. Flexure-based mecano-optical multi-degree-of-freedom transducers dedicated to medical force sensing instruments. <https://infoscience.epfl.ch/record/278197>, DOI: 10.5075/epfl-thesis-9628.
- [8] Robuschi, N., Braghin, F., Corigliano, A., Ghisi, A., and Tasora, A., 2017. “On the dynamics of a high frequency oscillator for mechanical watches”. *Mechanism and Machine Theory*, **117**, Nov., pp. 276–293, DOI: 10.1016/j.mechmachtheory.2017.07.013.
- [9] Thalmann, E., 2020. “Flexure Pivot Oscillators for Mechanical Watches”. PhD thesis, EPFL, Lausanne, DOI: 10.5075/epfl-thesis-8802.
- [10] Schneegans, H., Thalmann, E., and Henein, S., in press, 2021. “Shaking force balancing of a 2-DOF isotropic horological oscillator”. *Precision Engineering*.
- [11] Wittrick, W., 1948. “The Theory of Symmetrical Crossed Flexure Pivots”. *Australian Journal of Scientific Research A Physical Sciences*, **1**, May, p. 121.
- [12] Xu, Q., 2013. “Design and implementation of a novel rotary micropositioning system driven by linear voice coil motor”. *Review of Scientific Instruments*, **84**(5), May, p. 055001, DOI: 10.1063/1.4803187.
- [13] Henein, S., 2012. “Short Communication: Flexure delicacies”. *Mechanical Sciences*, **3**(1), Jan., pp. 1–4, DOI: 10.5194/ms-3-1-2012.

- [14] Cosandier, F., Henein, S., Richard, M., and Rubbert, L., 2017. *The Art of Flexure Mechanism Design*. EPFL Press, Lausanne, Switzerland.
- [15] Kahrobaiyan, M. H., Thalmann, E., Rubbert, L., Vardi, I., and Henein, S., 2018. “Gravity-Insensitive Flexure Pivot Oscillators”. *Journal of Mechanical Design*, **140**(7), May, pp. 075002–9, DOI: 10.1115/1.4039887.
- [16] Thalmann, E., Kahrobaiyan, M. H., Vardi, I., and Henein, S., 2020. “Flexure Pivot Oscillator With Intrinsically Tuned Isochronism”. *Journal of Mechanical Design*, **142**(7), July, DOI: 10.1115/1.4045388.
- [17] Thalmann, E., and Henein, S., 2021. “Optical Measurement Method for Mechanical Time Base Characterization”. In Euspen’s 21st International Conference & Exhibition.
- [18] Liu, L., Bi, S., Yang, Q., and Wang, Y., 2014. “Design and experiment of generalized triple-cross-spring flexure pivots applied to the ultra-precision instruments”. *Review of Scientific Instruments*, **85**(10), Oct., p. 105102, DOI: 10.1063/1.4897271.
- [19] Thalmann, E., and Henein, S., 2021. “Design of a Flexure Rotational Time Base With Varying Inertia”. *Journal of Mechanical Design*, **143**(11), Nov., p. 115001, DOI: 10.1115/1.4050558.
- [20] Ciblak, N., and Lipkin, H., 2003. “Design and Analysis of Remote Center of Compliance Structures”. *Journal of Robotic Systems*, **20**(8), pp. 415–427, DOI: 10.1002/rob.10096.
- [21] Pei, X., Yu, J., Zong, G., Bi, S., and Yu, Z., 2008. “Analysis of Rotational Precision for an Isosceles-Trapezoidal Flexural Pivot”. *Journal of Mechanical Design*, **130**(5), p. 052302, DOI: 10.1115/1.2885507.
- [22] Pei, X., Yu, J., Zong, G., Bi, S., and Hu, Y., 2009. “A Novel Family of Leaf-Type Compliant Joints: Combination of Two Isosceles-Trapezoidal Flexural Pivots”. *Journal of Mechanisms and Robotics*, **1**(021005), Jan., DOI: 10.1115/1.3046140.
- [23] Thalmann, E., and Henein, S., 2021. General TRIVOT kinematics animation [Video file], DOI: 10.5281/zenodo.4542221.
- [24] Grübler, M., 1917. *Getriebelehre: Eine Theorie Des Zwanglaufes Und Der Ebenen Mechanismen*. Springer-Verlag, Berlin Heidelberg.
- [25] Thalmann, E., and Henein, S., 2021. Symmetrical TRIVOT kinematics animation [Video file], DOI: 10.5281/zenodo.4553450.
- [26] Howell, L. L., Magleby, S. P., and Olsen, B. M., 2013. *Handbook of Compliant Mechanisms*. Wiley, Hoboken, NJ, DOI: 10.1002/9781118516485.
- [27] Thalmann, E., and Henein, S., 2021. TRIVOT: Triple Crossed Flexure Pivot [Video file], DOI: 10.5281/zenodo.4519424.
- [28] Haringx, J. A., 1949. “The cross-spring pivot as a structural element”. *Flow, Turbulence and Combustion*, **1**(1), Dec., p. 313, DOI: 10.1007/BF02120338.
- [29] Wittrick, W., 1951. “The properties of crossed flexure pivots, and the influence of the point at which the strips cross”. *The Aeronautical Quarterly*, **2**, Feb., pp. 272–292, DOI: 10.1017/S0001925900000470.
- [30] Zhao, H., and Bi, S., 2010. “Stiffness and stress characteristics of the generalized cross-spring pivot”. *Mechanism and Machine Theory*, **45**(3), pp. 378–391, DOI: 10.1016/j.mechmachtheory.2009.10.001.
- [31] Zhao, H., and Bi, S., 2010. “Accuracy characteristics of the generalized cross-spring pivot”. *Mechanism and Machine Theory*, **45**(10), pp. 1434–1448, DOI: 10.1016/j.mechmachtheory.2010.05.004.
- [32] ANSYS, 2018. ANSYS® Workbench, Release 19.2, ANSYS Workbench User’s Guide.
- [33] Thalmann, E., Kahrobaiyan, M. H., and Henein, S., 2018. “Flexure-Pivot Oscillator Restoring Torque Nonlinearity and Isochronism Defect”. In Proceedings of the ASME 2018 IDETC-CIE Conference, Vol. 5A, ASME, DOI: 10.1115/DETC2018-85863.
- [34] Zhang, A., Gou, Y., and Yang, X., 2020. Predicting Nonlinear Stiffness, Motion Range, and Load-Bearing Capability of Leaf-Type Isosceles-Trapezoidal Flexural Pivot Using Comprehensive Elliptic Integral Solution. <https://www.hindawi.com/journals/mpe/2020/1390692/>, DOI: 10.1155/2020/1390692.
- [35] Henein, S., 2000. “Conception des structures articulées à guidages flexibles de haute précision”. PhD thesis, EPFL, Lausanne, DOI: 10.5075/epfl-thesis-2194.
- [36] Henein, S., Barrot, F., Jeanneret, S., Fournier, R., Giriens, L., Gumy, M., Droz, S., and Toimil, M., 2011. “Silicon Flexures for the Sugar-Cube Delta Robot”. In Proceedings of the 11th Euspen International Conference, p. 4.
- [37] Bellouard, Y., 2011. “On the bending strength of fused silica flexures fabricated by ultrafast lasers”. *Optical Materials Express*, **1**(5), Sept., pp. 816–831, DOI: 10.1364/OME.1.000816.
- [38] Wheeler, B. A., 1957. Cross-spring flexure pivot, Patent Number: US2793028A.
- [39] Kiener, L., Saudan, H., Cosandier, F., Perruchoud, G., and Spanoudakis, P., 2019. “Innovative concept of compliant mechanisms made by additive manufacturing”. *MATEC Web of Conferences*, **304**, p. 07002, DOI: 10.1051/matec-conf/201930407002.